Applied Catalysis B: Environmental 90 (2009) 662–676

Contents lists available at ScienceDirect

Applied Catalysis B: Environmental

journal homepage: www.elsevier.com/locate/apcatb

Pt dispersion effects during NOx storage and reduction on Pt/BaO/Al_2O_3 catalysts☆

Robert D. Clayton [1], Michael P. Harold *, Vemuri Balakotaiah *, C.Z. Wan [2]

Department of Chemical & Biomolecular Engineering, University of Houston, S-222, Engineering Bldg 1, Houston, TX 77204-4004, United States

ARTICLE INFO

Article history:
Received 16 January 2009
Received in revised form 14 April 2009
Accepted 28 April 2009
Available online 6 May 2009

Keywords:
NOx
Hydrogen
Platinum
Dispersion
Barium
Selective catalytic reduction
NOx storage and reduction
Lean NOx trap

ABSTRACT

This study provides insight into the effect of Pt dispersion on the overall rate and product distribution during NOx storage and reduction. The storage and reduction performance of Pt/BaO/A_2O_3 monoliths with varied Pt dispersion (3%, 8%, and 50%) and fixed Pt (2.48 wt.%) and BaO (13.0 wt.%) loadings is reported. At low temperature (<200 °C), the differences in storage and reduction activity were the largest between the three catalysts. The amount of NOx stored increased with increased dispersion, as did the amount of stored NOx that was reduced. These trends are attributed to larger Pt surface area and Pt–BaO interfacial perimeter, the latter of which enhances the spillover of surface species between the precious metal and storage components. At high temperature (370 °C), the stored NOx was almost completely regenerated for the three catalysts. However, the regeneration of the 3% dispersion catalyst was much slower, suggesting a rate limitation involving the reverse spillover of stored NOx to Pt and/or of adsorbed hydrogen from Pt to BaO. The results indicate that the catalyst dispersion and operating conditions may be tuned to achieve the desired ammonia selectivity. For the aerobic regeneration feed, the most (net) NH_3 was generated by the 50% dispersion catalyst at the lowest temperature (125 °C), by the 3% dispersion catalyst at the highest temperature (340 °C), and by the 8% dispersion catalyst at the intermediate temperatures (170–290 °C). Similar trends were observed for the net production of NH_3 with an anaerobic regeneration feed. A phenomenological picture is proposed that describes the effects of Pt dispersion consistent with the established spatio-temporal behavior of the lean NOx trap.

1. Introduction

A promising technology for reducing NOx emissions in lean burn and diesel exhaust is the Lean NOx Trap (LNT), also known as the NOx Adsorber catalyst (NAC). The LNT operation involves periodic NOx storage and reduction (NSR). The engine is run under normal conditions with excess O_2 involved in the fuel combustion during the storage step. Then, for a shorter period, the engine is run rich or a reductant (fuel or reformed fuel) is injected into the exhaust gas during the regeneration step. The storage duration is of the order of a few minutes, while the regeneration duration is of the order of 1–10 s. The main components comprising the LNT are a NOx storage material such as an alkaline earth metal oxide (BaO), precious metals (Rh, Pt, Pd), and an oxygen storage material such as ceria (CeO_2). During the storage step, the role of the precious metals (Pd and Pt) is to oxidize NO to NO_2, which then reacts directly with the storage component, forming a mixture of nitrites and nitrates. During the regeneration step, the role of the precious metals (primarily Pt and Rh) is to selectively reduce the stored NOx to N_2.

The mechanism of regeneration of stored NOx is still not fully understood. Nova et al. [1,2] showed that the thermal decomposition of stored NOx was not necessary to reduce the stored NOx with H_2. They proposed that the reduction of stored nitrates involves a Pt-catalyzed surface reaction and argued that the pathway only occurs when both Pt and BaO are well dispersed on the same support. A study by Cant et al. [3] showed similar findings to Nova et al. [1] when comparing the results of a sample with Pt and BaO dispersed on the same support to those of a physical mixture of Pt and BaO on separate supports. In several studies, the reverse spillover of NOx from BaO to Pt is speculated to occur during the regeneration [3–8]. Cant et al. [3] concluded that the forward and reverse spillover of NOx is important since the exchange rate of ^{15}NO and stored ^{14}NOx during storage was more

* Corresponding authors.
E-mail addresses: Clayton_Robert_D@cat.com (R.D. Clayton), mharold@uh.edu (M.P. Harold), bala@uh.edu (V. Balakotaiah).
[1] Now with Caterpillar Inc., Peoria, IL, United States.
[2] BASF Catalysts LLC, Iselin, NJ 08830-0770, United States.

0926-3373/$ – see front matter © 2009 Elsevier B.V. All rights reserved.
doi:10.1016/j.apcatb.2009.04.029

than five times faster for the $Pt/BaO/Al_2O_3$ sample than for the physical mixture at 360 °C. James et al. [4] proposed a "reverse" spillover mechanism of NOx to explain the decomposition of nitrates stored far from Pt. Zhou et al. [7] have described the nitrate ions as being completely mobile on the barium phase with the reaction occurring at the Pt/Ba interface. The spillover of reductant from Pt to barium was proposed by Liu and Anderson [9]. The proposed mechanism involves the activation of reductant on Pt with subsequent spillover to the storage component where the reductant reacts directly with nitrates forming nitrites, which results in the release of the stored NOx as NO. However, debate still exists over the direction of spillover and the spillover species during the regeneration of stored NOx.

The storage of NOx has been studied in great detail with several mechanisms being proposed. NOx storage can occur not only on the BaO component but also on the γ-Al_2O_3 support [10–14]. The disproportionation mechanism is considered by most to be the dominant storage mechanism on BaO at long storage times (several minutes or more). The steps involve NO oxidation on Pt to NO_2 which stores directly on barium through a sequence of reactions [8,15–18]. The disproportionation mechanism requires three NO_2 molecules to form $Ba(NO_3)_2$, liberating one NO molecule. At long storage times, the stoichiometry was reported to be satisfied as long as NO_2 decomposition (on Pt) was not significant [19]. At short storage times the stoichiometry of 3 NO_2 to 1 NO was not observed in the presence of Pt. Epling et al. [20] suggested that the disproportionation mechanism occurred on BaO sites far from Pt whereas the initial storage of NOx occurred on storage sites in close proximity to Pt and involved oxygen adatoms. The oxygen adatoms on Pt were proposed to oxidize intermediate nitrites to nitrates [12,20]. Paterson et al. [12] also suggested that the spillover involved an activated form of NO_2 serving as an oxidant. Fridell et al. [21] proposed that oxygen adatoms enhanced the storage of NOx by a spillover mechanism. Similarly, Kabin et al. [15] proposed a third reaction pathway called a "hybrid" pathway in which oxygen adatoms on Pt spillover to BaO, which is followed by uptake of NO_2. Likewise, other proposed storage mechanisms require a close coupling of the Pt and BaO components [22,23]. Many groups have speculated that NOx storage can occur through the spillover of NOx from Pt to BaO [3,5,8,15]. Further, the stored NOx is proposed to have sufficient mobility to migrate from the surface to the bulk [12,13,24]. Finally, Sakamoto et al. [25] showed through a spatial imaging technique that the majority of NOx stores around the periphery of Pt particles situated on top of the storage component.

In spite of the established importance of the Pt–BaO coupling, the effect of the Pt particle size and dispersion has not been studied in detail for NOx storage and reduction. The Pt dispersion has been shown to be an important catalyst parameter during NO oxidation and was studied over Pt supported on Al_2O_3 and SiO_2 catalysts [26–30], which as described above is a very important step during the storage of NOx. These studies have shown that the turnover rate of NO oxidation increased with increased (decreased) Pt particle size (Pt dispersion). Olsson and Fridell [26] also studied $Pt/BaO/Al_2O_3$ catalysts with varied Pt dispersion and observed that an optimum Pt particle size exists for maximizing the amount of NO_2 produced. More recently, Lindholm et al. [31] showed that the NOx storage capacity depends on the method of preparation of the catalyst, specifically the order of deposition of the Pt and Ba on the washcoat.

The objective is to study the effect of the Pt dispersion on both NOx storage and stored NOx reduction. This is accomplished by systematically varying the dispersion of a $Pt/BaO/Al_2O_3$ monolith for fixed Pt and BaO loadings. Further, the effects of the exotherm and H_2O produced from H_2 oxidation during the regeneration of stored NOx with an aerobic regeneration feed are compared to the nearly isothermal (anaerobic) regeneration feed. The observed effects of Pt dispersion on the NOx conversion and product distribution are analyzed in terms of the established phenomological spatio-temporal behavior of the lean NOx trap.

2. Experimental

2.1. Catalyst samples

The catalyst samples were washcoated monolith catalysts provided by BASF Catalysts LLC (Iselin, NJ). The preparation procedure of the D series samples is described as follows. Catalyst B3 was prepared by a similar procedure highlighted below.

A commercially available γ-Al_2O_3 powder was impregnated with an aqueous solution containing a solubilized Pt amine complex (non-chloride containing preparation). After calcination at 500 °C in air, the alumina contained 3.35 wt.% Pt determined by ICP. The Pt dispersion was determined by pulse CO chemisorption technique to be 50%. The dispersion was verified by TEM and the Pt particles were not visible in XRD. The Pt containing powder was further impregnated with an aqueous barium acetate solution. After calcination at 500 °C in air, the Pt bearing alumina contained 15 wt.% BaO determined by ICP. TEM examination of the barium incorporated sample showed no indication of a change in the Pt dispersion. The size of the $Pt/Ba/\gamma$-Al_2O_3 powder particle was then reduced and a slurry was prepared. Additional uncatalyzed alumina was added to the slurry to form a final washcoat slurry to control the washcoat thickness on the cordierite monolith. The Pt and BaO content in the final washcoat on the monolith after 500 °C calcination were 2.48 wt.% and 12.7 wt.%, respectively determined by ICP. This monolithic sample containing 95 g/ft^3 monolith was designated as sample D50.

A portion of the aforementioned Pt/γ-Al_2O_3 powder prepared at 500 °C was subjected to oven aging at 700 °C for 2 h in air. The Pt dispersion was determined by pulse CO chemisorption technique to be about 8%. The dispersion was verified by TEM and XRD. XRD showed Pt particles around 125 Å in size by line broadening. The remaining procedure of Ba incorporation and washcoat preparation of the 700 °C aged Pt/γ-Al_2O_3 powder was identical to that of the D50 sample. This monolithic sample containing 95 g/ft^3 was designated as sample D8.

A portion of the aforementioned Pt/γ-Al_2O_3 powder prepared at 500 °C was subjected to oven aging at 800 °C for 5 h in air. The Pt dispersion was determined by pulse CO chemisorption technique to be around 3.2%. XRD showed Pt particles in excess of 300 Å in size. The remaining procedure of Ba incorporation and washcoat preparation of the 800 °C aged Pt/γ-Al_2O_3 powder was identical to that of the D50 and D8 samples. This monolithic sample containing 95 g/ft^3 was designated as sample D3.

The B3 sample was prepared by a slightly different preparation method. A γ-Al_2O_3 powder was impregnated with an aqueous solution containing the Pt amine complex. The impregnated powder was not calcined. The impregnated powder then was then milled with aqueous barium acetate solution to form a washcoat slurry. The final washcoated monolith after calcination at 500 °C was designated as sample B3. CO chemisorption was used to measure the Pt dispersion but was less reliable because of interference by barium.

The monolith samples were nearly cylindrical ($D \sim 0.8$ cm, $L = 2$ cm), containing Pt and BaO on a γ-alumina washcoat support coated on a cordierite structure (~62 channels/cm^2). The compositions and properties of the four catalyst types, D3, D8, D50, and B3, are provided in Table 1. The mass of washcoat material (m_{wc}) on each monolith piece was approximately 126 mg (D series) or 110 mg (B3). Assuming that the surface of the Pt particles is

Table 1
Catalysts used and their properties.

Sample	Pt (wt.%)	BaO (wt.%)	Pt dispersion (%)	Estimated Pt area (m^2 Pt/g w.c.)	Estimated Pt particle size (nm)	Measured Pt particle size (nm)	BET area (m^2/g)
B3	2.20	16.3	21.9	1.19	5.0	5.2	116
D50	2.48	13.0	50.0	2.90	2.2	–	–
D8	2.48	13.0	8.0	0.58	12.5	12.5	–
D3	2.48	13.0	3.2	0.17	31.3	30.0	–

smooth, the Pt particle size (nm) was estimated by the expression

$$d_{Pt} = \frac{1.1}{D_{Pt}} \times 100 \quad (1)$$

where D_{Pt} (%) is the Pt dispersion [32]. [Remark: For our case, Eq. (1) over-estimates the Pt particle size. The correct size was found to be better predicted with 1.1 in Eq. (1) replaced by 0.9.] The surface area of Pt per gram of washcoat (S_{Pt}) was derived by a first approximation that the Pt particles were shaped like hemispheres and is defined as

$$S_{Pt} = \frac{6}{d_{Pt}\rho_{Pt}}\left(\frac{m_{Pt}}{m_{wc}}\right) \quad (2)$$

where m_{Pt} and m_{wc} are the mass of Pt and washcoat and ρ_{Pt} is the bulk density of Pt.

Unless otherwise noted, the fresh catalyst samples were pre-treated under cycling conditions (20 cycles) at 400 °C with lean and rich cycles of 300 s and 60 s duration (except for the final cycle which had a rich duration of 300 s), respectively. The lean feed contained 500 ppm NO, 5% O_2, balance N_2 while the rich feed contained 1% H_2 in N_2. Any additional pre-treatment prior to each type of experiment is described below.

2.2. Flow reactor set-up

The NOx storage and reduction experiments were carried out with a flow reactor described in detail elsewhere [15,33–36]. To minimize bypassing, monoliths were wrapped in Fiberfrax® ceramic paper that had been heat treated before being placed in a quartz tube flow reactor. The effluent species from the reactor were analyzed by a quadrupole mass spectrometer and FT-IR [15,33]. The time delays for the QMS and FT-IR were accounted for in the concentration versus time plots by shifting the data corresponding to their respective time delays as estimated by inert pulsing experiments [34]. Some dispersion was observed to occur in the effluent lines, slightly affecting the concentration profiles [35]. The feed, effluent, and monolith temperatures were measured by thermocouples positioned 1 cm upstream and downstream of the monolith and at the geometric midpoint of the monolith [33,36]. For the experiments with an aerobic regeneration feed, the monolith temperature was measured at the front end of the monolith (approximately 0.2 cm from the inlet) where the temperature rise is the largest [33].

2.3. NO storage experiments

Prior to the storage experiments, a conditioning process was imposed to maximize reproducibility from run to run over the course of the study. This procedure included a minimum of 15 cycles of alternating lean and rich feeds until a cyclic steady-state was reached at the particular inert feed temperature of the storage experiment. The inert feed temperature is the feed gas temperature to the reactor under non-reactive conditions (Ar only) [35]. The lean feed had a 60 s duration and contained 500 ppm NO and 5% O_2 while the rich feed was 10 s long and contained 0.5% O_2 and 2% H_2 for the conditioning process. It is known that the NOx trap is not completely regenerated during actual cyclic operation. Thus, the presence of residual stored NOx prior to the storage experiments is more realistic than starting with a completely regenerated catalyst. The residual stored NOx will reduce the NOx storage capacity of the LNT at long storage times compared to a completely reduced catalyst prior to storage. After this conditioning procedure, pure Ar was flowed over the catalyst for 5 min to cool the monolith down to the desired inert feed temperature. This ensured that the monolith temperature was constant throughout the ca. 120 s storage experiment. The total NOx stored (moles/g washcoat) was calculated by

$$NOx^{stored}(t_S) = \frac{\int_0^{t_S}[F^o_{NO} - F_{NOx}(t)]\,dt}{m_{wc}} \quad (3)$$

where t_S is the storage time and F_i is the molar flow rate of species i. Note that Eq. (3) will slightly over-estimate the amount of NOx stored during cycling at low temperatures due to NH_3 or NHx species formed during the regeneration of the NOx trap that are retained by the catalyst and that react with NO and O_2 during the subsequent storage step [10,33].

2.4. Lean and rich cycling experiments

For the cycling experiments, the storage step comprised a feed containing 500 ppm NO and 5% O_2 in Ar (60 s), while the rich pulse contained 2% H_2 and 0.5% O_2 in Ar (10 s) at a total flow rate of 1000 sccm (GHSV = 60,000 h^{-1}). The rich pulse composition corresponded to a pulse stoichiometric number ($S_{N,p}$) of 0.5 where $S_{N,p} = (2[O_2] + [NO])/[H_2]$. The "excess" H_2 was essentially 1%, i.e., excess $H_2 = [H_2] - 2[O_2] - [NO]$, which assumes that all of the O_2 in the rich pulse reacts with H_2 to form H_2O. [Remark: the low but nonzero O_2 concentration in the rich pulse corresponds to the case when reductant is added to the exhaust gas or incomplete O_2 consumption occurs during the rich combustion in the engine.] The cycle-averaged results were obtained over at least five cycles after the system had reached a cyclic steady-state. Catalyst activity (Pt dispersion) changes were minimized by ensuring that the catalyst temperature did not exceed 425 °C. The cycle-averaged NOx conversion was calculated by

$$X_{NOx} = \frac{\int_0^{t_{S+R}}\left[F^o_{NO}(t) - F_{NOx}(t)\right]dt}{\int_0^{t_{S+R}} F^o_{NO}(t)\,dt} \quad (4)$$

where t_{S+R} (s) time for one complete lean and rich cycle, F_i^o (moles/s) is the feed rate of species i, and F_i (moles/s) is the effluent molar flow rate of species i.

2.5. NO oxidation experiments

A mixture containing 500 ppm NO and 5% O_2 in Ar was fed to the reactor until the effluent NOx ($NO + NO_2$) concentration was within 3% of the feed NO concentration. The time for the NO oxidation reaction to reach a steady-state was dependent on the

time needed for the barium storage phase to become saturated with NOx. Muncrief et al. [37] used a TGA to measure the weight change of a Pt/BaO catalyst while storing NOx with a feed of NO/O_2. They observed that the catalyst continued to store NOx for more than 20 h with only a fraction of the barium utilized. Therefore, instead of waiting that long, the remaining 3% of the NO fed that was unaccounted for (485 ppm < effluent NO + NO_2 < 500 ppm) was assumed to be converted to NO_2 and stored on the catalyst.

2.6. Fixed NOx storage experiments

The amount of NOx stored with a feed of 500 ppm NO and 5% O_2 in Ar was fixed at 1.5×10^{-5} moles for some of the experiments involving the D series catalysts. The procedure ensured that the starting storage value was within 4% of the 1.5×10^{-5} value. It was initiated by exposing the catalyst at elevated temperature in 1% H_2 prior to each experiment. This was carried out until H_2O and NH_3 were not observed in the effluent. In order to avoid Pt sintering of the D50 catalyst, the pre-treatment temperature was limited to 425 °C. Catalysts D3 and D8 were heated to 500 °C in 1% H_2 to ensure that the catalysts were regenerated. After this pre-treatment, the catalyst sample was cooled to the desired temperature in a flow of Ar. A storage experiment was then conducted (500 ppm NO and 5% O_2). The duration of this initial storage process was set at 120 s and was carried out to estimate the storage time required to give 1.5×10^{-5} moles of stored NOx for each of the three catalyst samples. This procedure (pre-treatment and storage) was repeated at four temperatures (160 °C, 230 °C, 300 °C, and 370 °C). After the storage times were determined for the four temperatures, the catalysts were again pre-treated and cooled in flowing Ar to the desired temperature before running each storage (pre-determined time) and reduction (200 s) experiment at each temperature. Two additional experiments were conducted for catalyst D3 in which the regeneration conditions were aerobic (1.15% H_2 and 0.5% O_2, excess H_2 = 1500 ppm). The pre-treatment feed was changed for the aerobic experiments from anaerobic conditions (1% H_2) to aerobic conditions (2% H_2 and 0.5% O_2) at 425 °C. The pre-treatment was run until NH_3 and H_2O were not observed in the effluent (approximately 300 s).

Since the fixed stored NOx experiments involved only one cycle, the NOx conversion was based on the amount of the initial NOx stored that reacted. The stored NOx conversion for the complete regeneration was calculated from the expression

$$X_{\mathrm{NOx\,stored}} = \frac{\int_0^{t_R} [F_{\mathrm{NOx}}(t) + F_{\mathrm{NH_3}}(t) + 2(F_{\mathrm{N_2O}}(t) + F_{\mathrm{N_2}}(t))]\,dt + [\mathrm{NHx^{acc}}]_{t_R}}{\int_0^{t_S} [F^{o}_{\mathrm{NO}} - F_{\mathrm{NOx}}(t)]\,dt} \times 100 \tag{5}$$

where t_R is the regeneration time. The denominator is the amount of NOx stored (moles) and was fixed (1.5×10^{-5}). The F_{NOx} term in the numerator is NOx that was stored and then released as NO and NO_2 (''NOx puff'') during the regeneration. Although the ''NOx puff'' represents unconverted NOx, the storage sites are converted back to $Ba(OH)_2$ and BaO. The $[NHx^{acc}]_{t_R}$ (moles) is the amount of NHx species (predominantly in the form of NH_3) on the catalyst at the end of the regeneration which converts to N_2 and N_2O during the subsequent O_2 treatment [33]. The amount of NH_3 accumulated on the catalyst during the regeneration was estimated by flowing a mixture of 5% O_2 in Ar over the sample after the 200 s regeneration and measuring the N_2 and N_2O formed; it is given by

$$[\mathrm{NHx^{acc}}]_{t_R} = 2\int_0^{t_S} [F_{\mathrm{N_2O}}(t) + F_{\mathrm{N_2}}(t)]\,dt \tag{6}$$

The corresponding selectivities for the entire regeneration are defined as

$$S_{\mathrm{NH_3}} = \frac{\int_0^{t_R} F_{\mathrm{NH_3}}(t)\,dt}{\int_0^{t_R} F_{\mathrm{NOx}}(t) + F_{\mathrm{NH_3}}(t) + 2(F_{\mathrm{N_2O}}(t) + F_{\mathrm{N_2}}(t))\,dt + [\mathrm{NHx^{acc}}]_{t_R}} \times 100\% \tag{7a}$$

$$S_{\mathrm{N_2O}} = \frac{2\int_0^{t_R} F_{\mathrm{N_2O}}(t)\,dt}{\int_0^{t_R} [F_{\mathrm{NOx}}(t) + F_{\mathrm{NH_3}}(t) + 2(F_{\mathrm{N_2O}}(t) + F_{\mathrm{N_2}}(t))]\,dt + [\mathrm{NHx^{acc}}]_{t_R}} \times 100\% \tag{7b}$$

$$S_{\mathrm{N_2}} = \frac{2\int_0^{t_R} F_{\mathrm{N_2}}(t)\,dt}{\int_0^{t_R} [F_{\mathrm{NOx}}(t) + F_{\mathrm{NH_3}}(t) + 2(F_{\mathrm{N_2O}}(t) + F_{\mathrm{N_2}}(t))]\,dt + [\mathrm{NHx^{acc}}]_{t_R}} \times 100\% \tag{7c}$$

The instantaneous stored NOx conversion at time t^* during the regeneration was calculated from only the species exiting the monolith (Eq. (5) with $t_R = t^*$ and without accounting for $[NHx^{acc}]_{t^*}$). The $[NHx^{acc}]_{t^*}$ term was only taken into account in these calculations for $t^* = t_R = 200$ s. At the end of each regeneration ($t^* = t_R = 200$ s), a gas mixture containing 5% O_2 in Ar was fed to the reactor producing N_2 and N_2O. The effluent N_2 and N_2O produced from the oxidation of the NH_3 (NHx species) was used to estimate the amount of NHx species retained by the catalyst by the end of the regeneration [10,33]. However, due to the retention of NHx species by the catalyst as the H_2 front moves along the monolith length, the calculated instantaneous stored NOx conversion is an under-estimate at low temperature since the effluent species are the only species considered.

3. Experimental results

3.1. NOx storage and NO oxidation

In order to quantify the effect of Pt dispersion on NOx storage, a series of experiments were conducted with catalyst samples D3, D8, and D50 to quantify the effect of Pt dispersion on NOx storage. The results are reported in Fig. 1 over a range of temperatures (125–350 °C) for 60 s and 120 s of exposure to a feed gas containing 500 ppm NO and 5% O_2 in Ar. The results show that as the temperature was increased, the amount of NOx stored increased for each catalyst. In addition, the amount of NOx stored increased with increased Pt dispersion for each temperature. Table 2 reports the ratio of NOx stored between the varied Pt dispersion catalysts ([NOx stored]$_{50\%}$/[NOx stored]$_{8\%}$ and [NOx stored]$_{8\%}$/[NOx stored]$_{3\%}$) for 60 s storage time. The ratios are highest at low temperature (125 °C) and decrease with temperature. At the highest temperature (350 °C), there is a negligible difference (approximately 10%) in the amount of NOx stored.

The dependence of the steady-state conversion of NO to NO_2 on the monolith temperature and Pt dispersion are shown in Fig. 2. The feed consisted of 500 ppm NO and 5% O_2 in Ar. A maximum in the NO conversion was observed between 270 °C and 330 °C, the exact value of which depended on the catalyst. Catalyst B3 (intermediate Pt dispersion) was the most active of the four catalysts, while D3 (lowest Pt dispersion) was the least active. The data show that the NO conversion maximum itself exhibits a maximum with respect to Pt particle size and exposed Pt atoms.

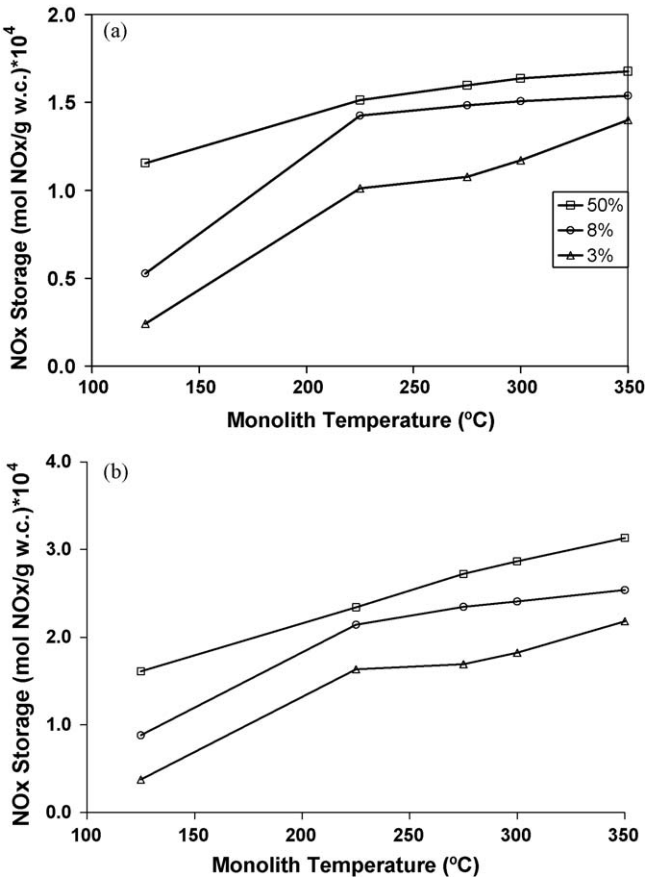

Fig. 1. NOx storage as a function of temperature on the D series catalysts: (a) 60 s; (b) 120 s [500 ppm NO and 5% O_2, balance Ar (varied)].

3.2. NOx storage and reduction

Cycle-averaged NOx conversions and product selectivities are reported in Fig. 3 for the varied dispersion catalysts (D series). The aerobic regeneration feed consisted of 2% H_2 and 0.5% O_2 in Ar and had a duration of 10 s. All of the selectivity and NOx conversion trends observed in Fig. 3a (50% dispersion) are consistent with results reported previously by Clayton et al. [10,33] for Pt/BaO catalysts having dispersions of 21.9% and 33% and temperatures up to 350 °C. For example, the NOx conversion and N_2 selectivity both increase with temperature, while the NH_3 and N_2O selectivity are highest at the lowest temperature. In the current study, experiments were not conducted above 350 °C in order to minimize deactivation (Pt sintering); as a result, the decrease in NOx conversion and N_2 selectivity and increase in NH_3 selectivity at higher temperatures reported in Refs. [10,33] were not observed here. For all three Pt dispersions, the NOx conversion increased and N_2O selectivity decreased with increased temperature. The NH_3 selectivity decreased monotonically with temperature from 60% at

Table 2
The ratio of NOx stored between the varied Pt dispersion catalysts ($[NOx\ stored)]_{50\%}/[NOx\ stored]_{8\%}$ and $[NOx\ stored)]_{8\%}/[NOx\ stored]_{3\%}$) for 60 s of storage [500 ppm NO, 5% O_2, balance Ar].

Temperature (°C)	50%/8%	8%/3%
125	2.10	2.27
225	1.06	1.41
275	1.08	1.38
300	1.09	1.29
350	1.09	1.10

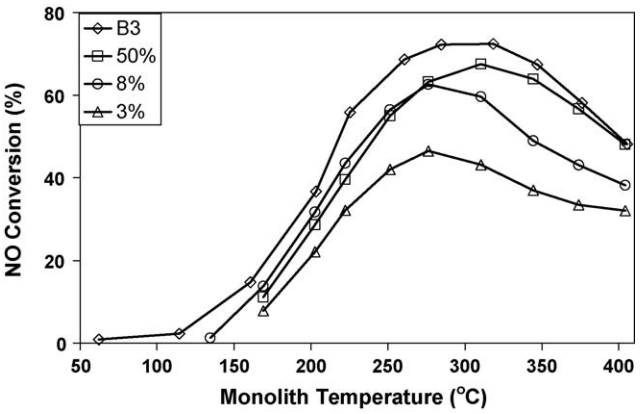

Fig. 2. Effect of Pt dispersion on NO oxidation on the D series and B3 catalysts [500 ppm NO and 5% O_2, balance Ar].

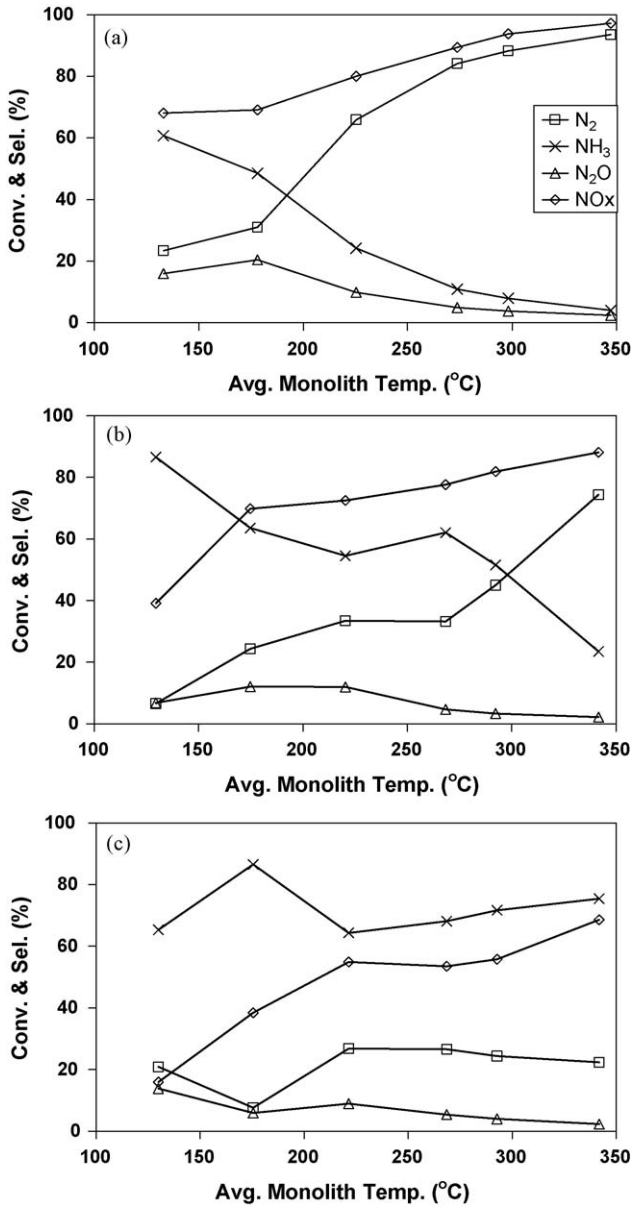

Fig. 3. Cycle-averaged conversions and selectivities as a function of temperature on the D series catalysts: (a) D50 (50%); (b) D8 (8%); (c) D3 (3%) [lean: 500 ppm NO, 5% O_2, balance Ar (60 s); rich: 2% H_2, 0.5% O_2, balance Ar (10 s)].

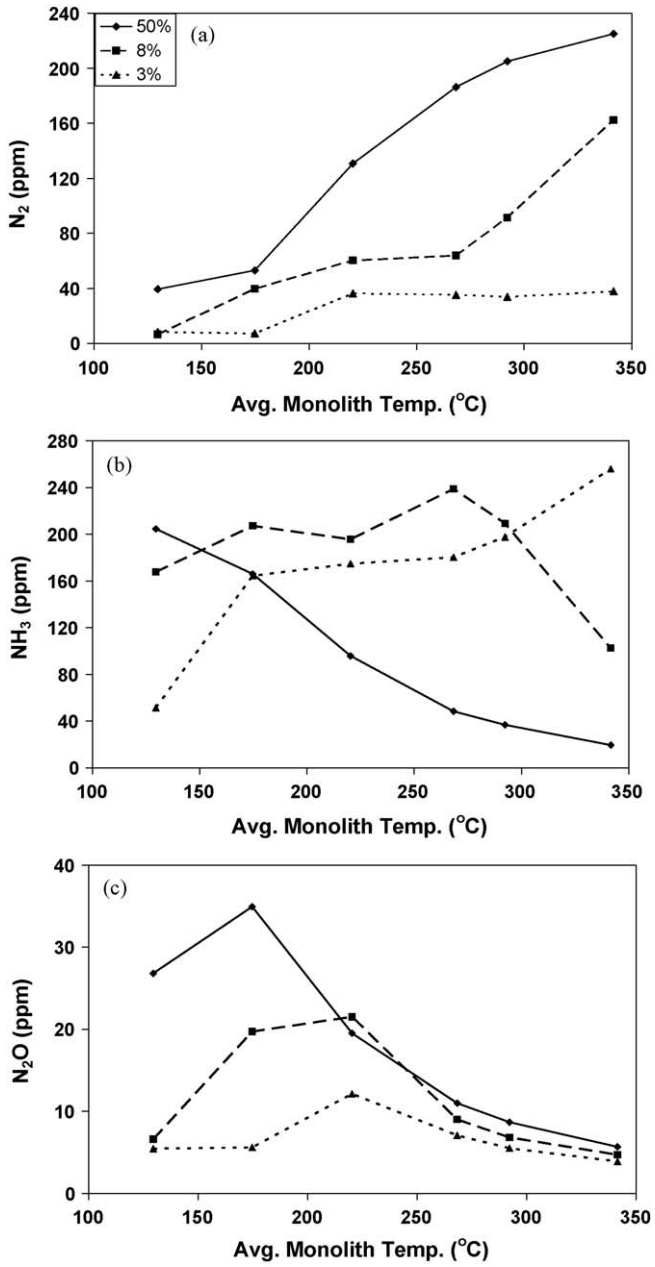

Fig. 4. Cycle-averaged concentrations as a function of temperature on the D series catalysts: (a) N_2; (b) NH_3; (c) N_2O [lean: 500 ppm NO, 5% O_2, balance Ar (60 s); rich: 2% H_2, 0.5% O_2, balance Ar (10 s)].

125 °C to less than 5% at 350 °C for catalyst D50, while for catalyst D3 the NH_3 selectivity exceeded 60% for all of the temperatures studied with a maximum observed at 175 °C. The NH_3 selectivity for the D3 catalyst exhibited a shallow maximum and minimum at 175 °C (86%) and 225 °C (64%), respectively. Catalyst D8 exhibited the highest selectivity to NH_3 (nearly 90%) at 125 °C, although the NOx conversion was only 40%. The N_2 selectivity trends for the three catalysts were roughly equal to $100 - S_{NH_3}$ (%) since the N_2O selectivity was low and only changed slightly with temperature.

In Fig. 4, the cycle-averaged effluent concentrations of N_2, NH_3, and N_2O are reported as a function of the cycle-averaged monolith temperature. For each catalyst, the N_2 concentration increased with monolith temperature. For catalyst D50, the N_2 concentration increased the most over the temperature range studied, while for catalyst D3 the N_2 concentration increased only slightly. Interestingly, catalyst D50 produced the most net NH_3 at the lowest temperature (125 °C) studied, catalyst D3 produced the most net NH_3 at the highest temperature (340 °C) studied, while catalyst D8 produced the most net NH_3 in the intermediate temperature range (170–290 °C). The net NH_3 produced from D50 (D3) decreased (increased) with temperature while catalyst D8 had a maximum in net NH_3 production at 270 °C. The production of N_2O was comparatively low for the three catalysts with the most N_2O produced (ca. 35 ppm) at 125 °C for D50.

Experiments were conducted with a fixed amount of stored NOx in order to isolate the regeneration performance from the storage capacity over a range of temperatures. The regeneration feed consisted of 1500 ppm excess H_2 (anaerobic: 1500 ppm H_2 in Ar; aerobic: 1.15% H_2 and 0.5% O_2 in Ar) and was fed to the reactor for a duration of 200 s. Fig. 5 shows typical effluent concentration profiles of total NOx, N_2, N_2O, NH_3, and H_2, during the first 100 s of the regeneration for catalyst D8. At the onset of the regeneration, the effluent NOx concentration slowly decreased from its level at the end of the storage. Both N_2 and N_2O abruptly appeared at the onset of the regeneration. Only small amounts of N_2O were formed due to the high temperature (370 °C). The N_2 effluent profile reached a maximum of 290 ppm and maintained that concentration level for about 20 s and then began to decrease as H_2 and NH_3 breakthrough commenced. The inset of Fig. 5 shows that H_2 and NH_3 breakthrough occurred nearly simultaneously. Shortly after breakthrough, H_2 monotonically approached the feed H_2 concentration, while NH_3 initially increased and then decreased as the stored NOx was depleted. These trends reported for the 8% dispersion catalyst are typical for the other two catalysts.

The stored NOx conversions (determined by Eq. (5)) and product selectivities (Eq. (7)) during the fixed stored NOx experiments are shown in Fig. 6 over a range of temperatures. The NOx conversion increased with temperature for all the three catalysts. The N_2O selectivity was negligible (<7%) under these conditions. The NH_3 selectivity decreased monotonically with temperature for catalysts D50 and D3. For D50, the NH_3 selectivity decrease was more significant; from a maximum value of 55 to 5%, while for D3 the decrease was from 90% to 83% over the same temperature range. For catalyst D8, the NH_3 selectivity decreased from 81% to 62% between 160 °C and 230 °C, stayed essentially constant from 230 °C to 300 °C, and then decreased sharply from 300 °C to 370 °C.

Whether the stored NOx is regenerated before or after H_2 breakthrough provides information about the rate limiting process. Table 4 reports the estimated percentage of stored NOx regenerated before and after H_2 breakthrough for the D series

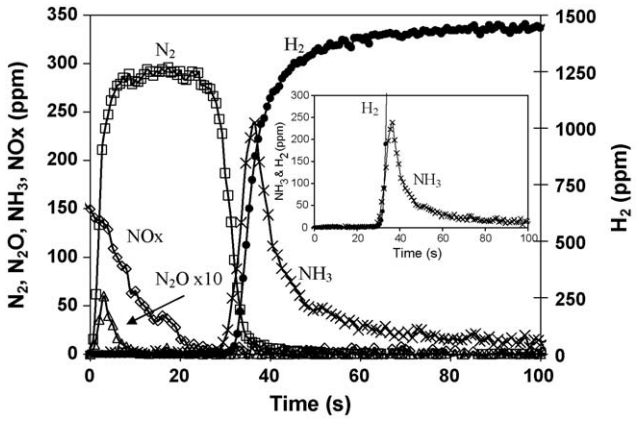

Fig. 5. Effluent concentration profiles of NOx, N_2, N_2O, NH_3, and H_2 during the regeneration, for a fixed amount of NOx stored (1.5×10^{-5} moles NOx) on catalyst D8 at 370 °C [lean: 500 ppm NO, 5% O_2, balance Ar (varied); rich: 1500 ppm H_2, balance Ar (200 s)].

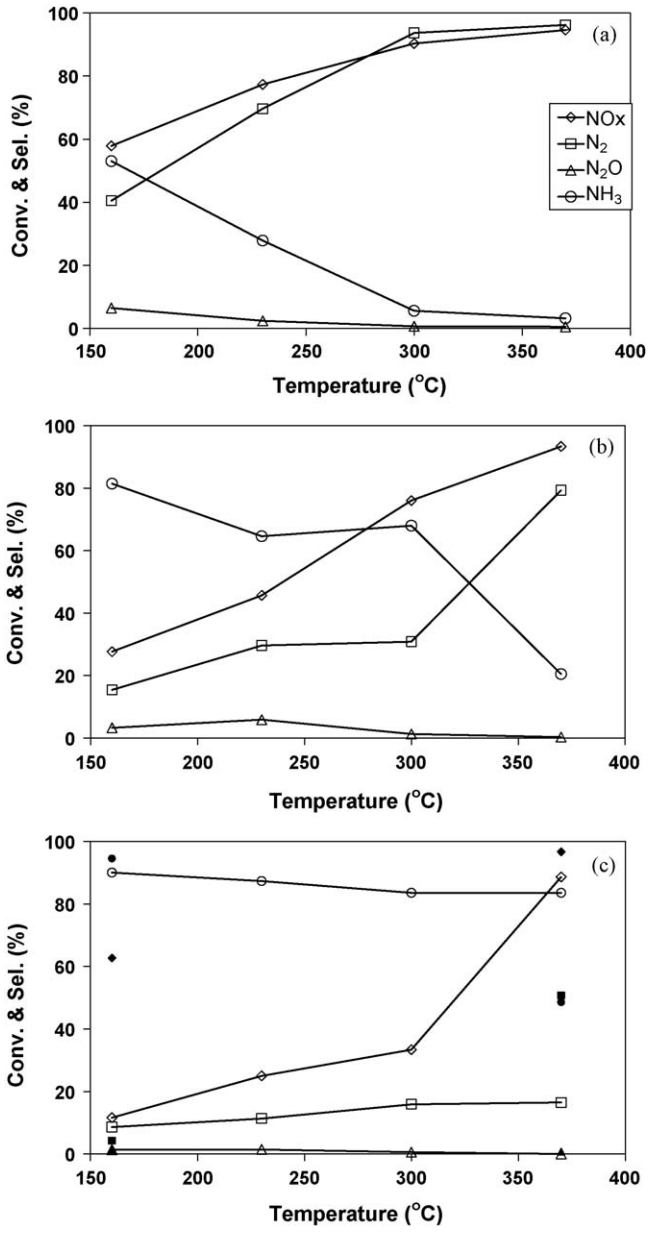

Fig. 6. Conversions and selectivities as a function of temperature for a fixed amount of NOx stored (1.5×10^{-5} moles NOx) on the D series catalysts: (a) D50 (50%); (b) D8 (8%); (c) D3 (3%) [lean: 500 ppm NO, 5% O_2, balance Ar (varied); rich: 1500 ppm H_2 (anaerobic, open symbols) or 1.15% H_2 and 0.5% O_2 (aerobic, solid symbols) balance Ar (200 s)].

catalysts. The percentage of stored NOx regenerated after H_2 breakthrough for catalyst D3 exceeded 80% over the temperature range studied. Catalysts D8 and D50 regenerated the lowest fraction of stored NOx prior to H_2 breakthrough at the lowest temperature (160 °C) and the most at the highest temperature (370 °C). These results will be analyzed in the next section in the context of rate limiting processes.

In Fig. 7, the net NH_3 produced is reported for the three catalysts at four different feed temperatures. For the anaerobic regeneration and lowest feed temperature (160 °C), catalyst D50 produced the most net NH_3, followed by D8 and then D3. However, for the aerobic regeneration, catalyst D3 produced more net NH_3 than the other catalysts under anaerobic conditions. At intermediate feed temperatures (230 °C and 300 °C), catalyst D8 produced the most net NH_3, while at 370 °C catalyst D3 produced the most net NH_3. Unlike the results at 160 °C, at 370 °C catalyst D3 produced more

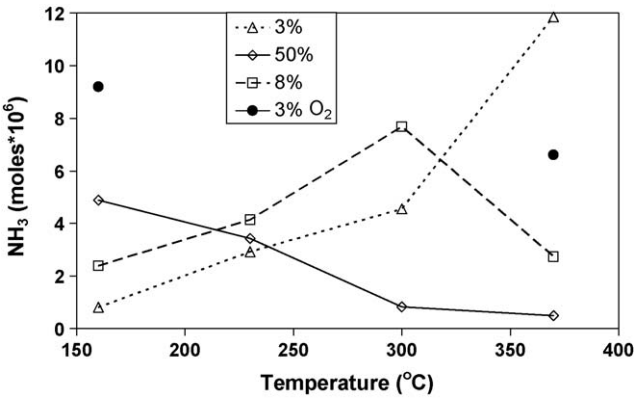

Fig. 7. Net NH_3 formed as a function of temperature for a fixed amount of NOx stored (1.5×10^{-5} moles NOx) on the D series catalysts [lean: 500 ppm NO, 5% O_2, balance Ar (varied); rich: 1500 ppm H_2 (anaerobic, open symbols) or 1.15% H_2 and 0.5% O_2 (aerobic, solid symbols) balance Ar (200 s)].

net NH_3 during the anaerobic regeneration than during the aerobic regeneration.

During the aerobic regeneration some of the H_2 is oxidized so it is important to quantify the extent of the exotherm. The monolith temperature rise during the regeneration for the fixed stored NOx experiments are reported in Fig. 8. During the anaerobic regeneration, the monolith temperature increased only slightly (4–5 °C) at the onset of the regeneration and then decreased back down to the initial monolith temperature prior to the regeneration. Effectively, these experiments are isothermal. On the other hand, during the aerobic regeneration (0.5% O_2 and 1.15% H_2) the monolith temperature increased approximately 75 °C at the front end during the regeneration for the two experiments with a feed temperature of 160 °C and 370 °C. Theis and Gulari [38] inferred the temperature of the precious metal sites to be 130 °C higher than that of the exhaust gas exiting the LNT. Therefore, measuring the temperature inside a monolith channel does not give the actual temperature of the precious metal.

The results for the fixed NOx storage experiments are plotted in the form of instantaneous stored NOx conversion in Fig. 9. As the Pt dispersion increased, the amount of stored NOx that was regenerated during the entire regeneration increased during the anaerobic regenerations. However, the extent of NOx conversion achieved at 200 s was a sensitive function of the feed temperature. At 370 °C (Fig. 9d), all three catalysts approached 100% instanta-

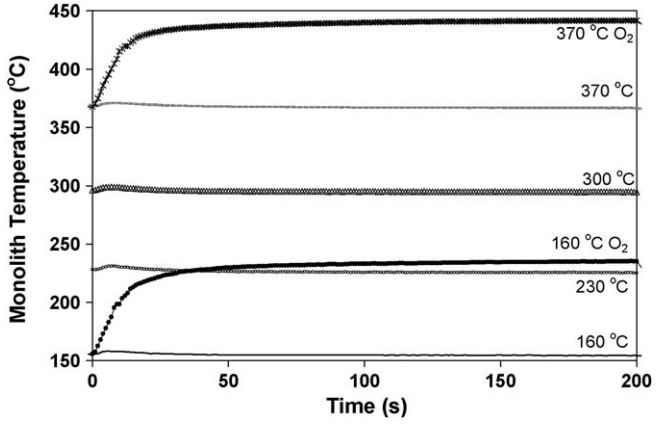

Fig. 8. Monolith temperature during the regeneration for the fixed amount of NOx stored (1.5×10^{-5} moles NOx) experiments on catalyst D3 [lean: 500 ppm NO, 5% O_2, balance Ar (varied); rich: 1500 ppm H_2 or 1.15% H_2 and 0.5% O_2 balance Ar (200 s)].

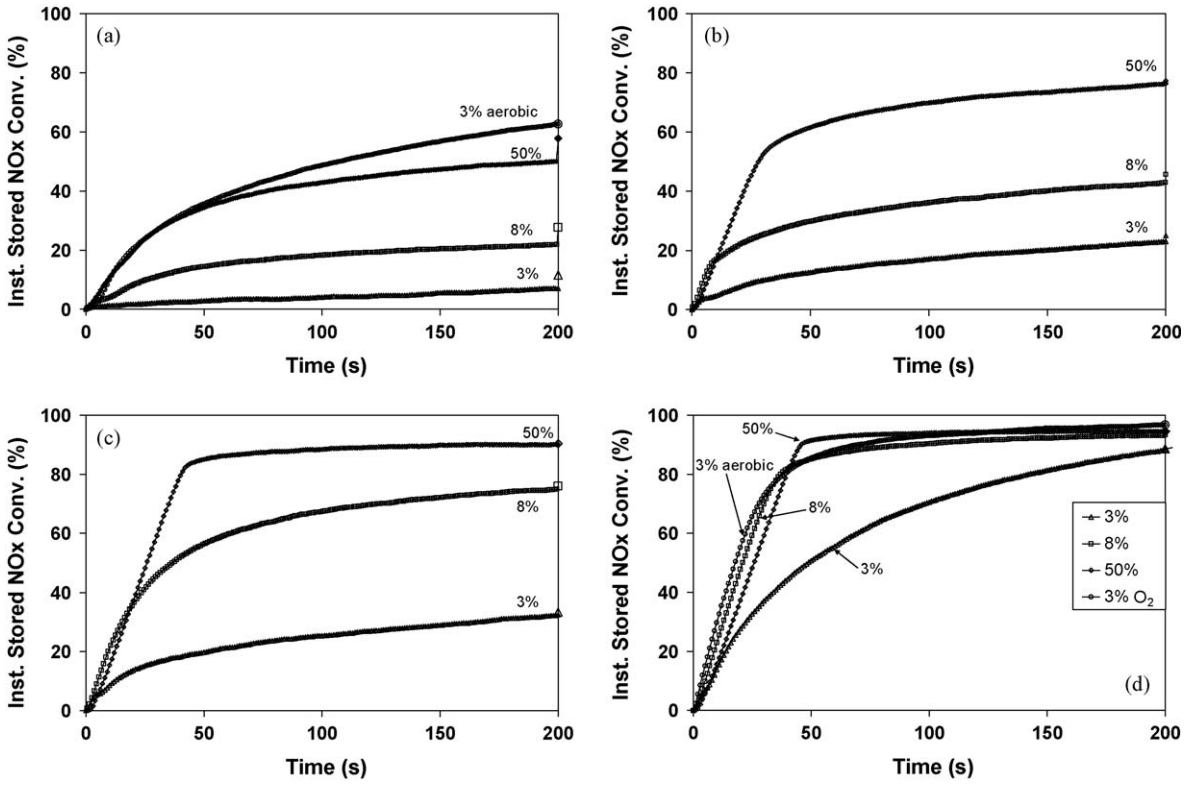

Fig. 9. Instantaneous stored NOx conversion as a function of time for a fixed amount of NOx stored (1.5×10^{-5} moles NOx) on the D series catalysts: (a) 160 °C; (b) 230 °C; (c) 300 °C; (d) 370 °C [lean: 500 ppm NO, 5% O_2, balance Ar (varied); rich: 1500 ppm H_2 or 1.15% H_2 and 0.5% O_2, balance Ar (200 s)].

neous NOx conversion prior to the end of the 200 s regeneration. In contrast, at 160 °C the highest instantaneous conversion was 50% for catalyst D50 under anaerobic conditions. Moreover, the rate of conversion of stored NOx (slope of curve) to complete conversion varied. For example, the rate of conversion was the slowest for D3 when the feed was anaerobic. The presence of O_2 during the regeneration also had a noted effect. At 160 °C, the aerobic regeneration of catalyst D3 was more effective in regenerating the stored NOx than the anaerobic feed. At the end of each anaerobic regeneration (200 s), 5% O_2 was added to the Ar feed gas. This resulted in the production of N_2 and N_2O produced from the reactions:

$$R_1: \quad \mathrm{NHx} + \frac{x}{4}\mathrm{O_2} \xrightarrow{\mathrm{Pt}} \frac{1}{2}\mathrm{N_2} + \frac{x}{2}\mathrm{H_2O}$$

$$R_2: \quad \mathrm{NHx} + \left(\frac{1}{4} + \frac{x}{4}\right)\mathrm{O_2} \xrightarrow{\mathrm{Pt}} \frac{1}{2}\mathrm{N_2O} + \frac{x}{2}\mathrm{H_2O}$$

The N_2 and N_2O produced after the regeneration are shown by the jump in instantaneous stored NOx conversion at 200 s (Fig. 9a). As the temperature increased, the amount of N_2 and N_2O formed decreased due to an increased rate of NH_3 desorption (compare Fig. 9a to b–d).

The measured effluent concentrations of H_2 and NH_3 for the set of fixed NOx storage experiments are shown in Figs. 10 and 11. The breakthrough time of H_2 during the regeneration increased with increasing Pt dispersion for all of the temperatures studied. For the 3% dispersion catalyst, H_2 breakthrough occurred earlier for the anaerobic regeneration feed than for the aerobic regeneration feed at both temperatures (160 °C and 370 °C). For all the three catalysts, the breakthrough time of H_2 and NH_3 increased with increasing feed temperature. In all cases, the breakthrough of H_2 and NH_3 occurred within 2 s of each other. Upon breakthrough of H_2 for the 160 °C and 230 °C anaerobic feed experiments (Fig. 10a and b), the H_2 effluent concentration increased the fastest to the inlet H_2 concentration level for catalyst D3 and the slowest for catalyst D50. At 370 °C (Fig. 10d), the trend was the opposite. Catalyst D50 had the steepest effluent H_2 profile, while the effluent H_2 concentration profile for catalyst D3 approached the feed H_2 concentration much more slowly. As seen in Fig. 11, once NH_3 appeared in the effluent, its effluent concentration initially increased rapidly to a maximum value before slowly decreasing. At 160 °C, NH_3 formation was not observed for catalyst D3 (Fig. 11d).

4. Analysis and discussion

In this study, the effect of Pt dispersion on the performance of a Pt/BaO/alumina coated monolith was determined through a systematic set of transient experiments. Previous studies reported the overall performance of the lean NOx trap using a Pt/BaO monolith catalyst and H_2 as the reductant [10,33,34,36]. The data reported here provide more information about Pt particle size effects and insight on Pt/BaO interfacial coupling. The LNT experiments were carried out under integral operation (high cycle-averaged NOx conversion) with varying extent of non-isothermality and transport limitations. Earlier experimental and modeling studies of NOx reduction in LNT catalysts have assessed the importance of nonisothermal effects, transverse mass transport, and washcoat diffusion during NOx storage and reduction [39,40]. For example, the extent of nonisothermal behavior is mainly determined by the concentration of O_2 during the regeneration step [34]. Moreover, traveling fronts of concentration and temperature are present during conventional LNT operation while external mass transfer and washcoat diffusion may be present especially during NOx reduction [33,39,40]. The manifestation of these processes for the catalysts of varied dispersion are examined in this study.

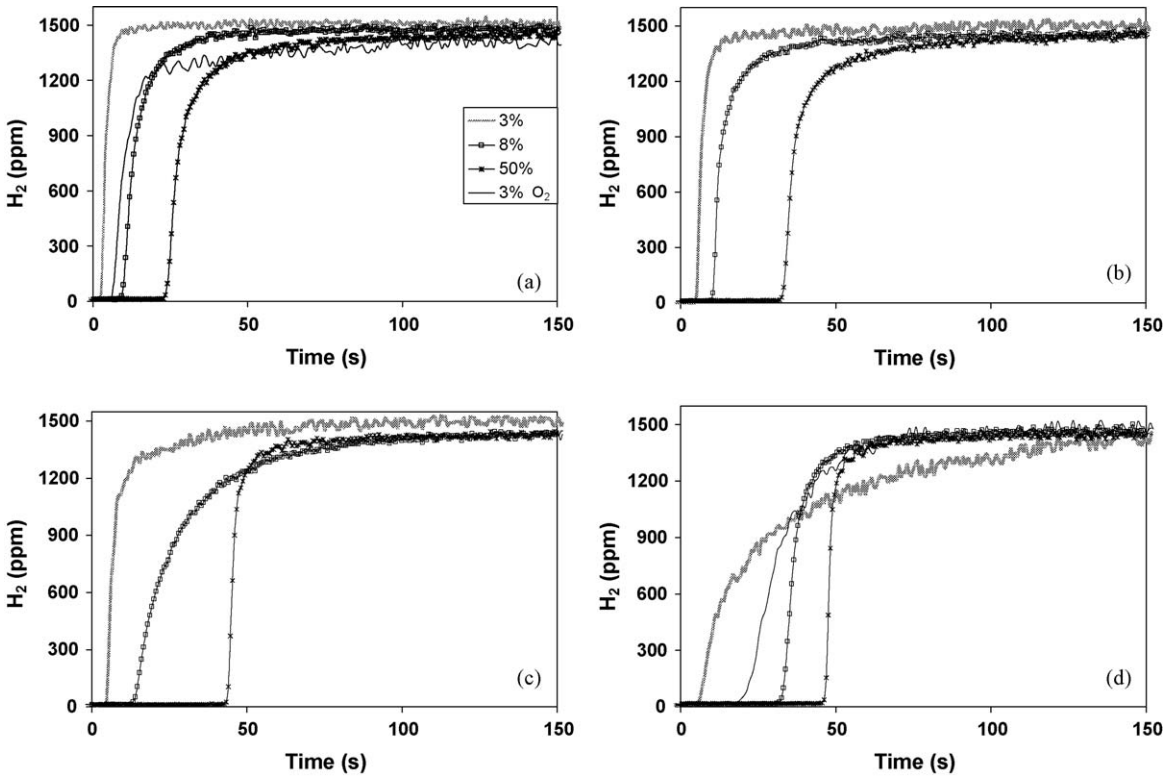

Fig. 10. Effluent H_2 concentration during the regeneration of a fixed amount of NOx stored (1.5×10^{-5} moles NOx) on the D series catalysts: (a) 160 °C; (b) 230 °C; (c) 300 °C; (d) 370 °C [lean: 500 ppm NO, 5% O_2, balance Ar (varied); rich: 1500 ppm H_2 or 1.15% H_2 and 0.5% O_2, balance Ar (200 s)].

4.1. NOx storage and NO oxidation

The NOx storage results reported here are consistent with previous studies with respect to the temperature dependence of NOx stored. However, the specific effect of the Pt dispersion, not reported in previous studies, reveals the important role of Pt and associated spillover processes. Whether the spillover from the precious metal (Pt) to storage phase (BaO) involves NO_2 [8,16], NO

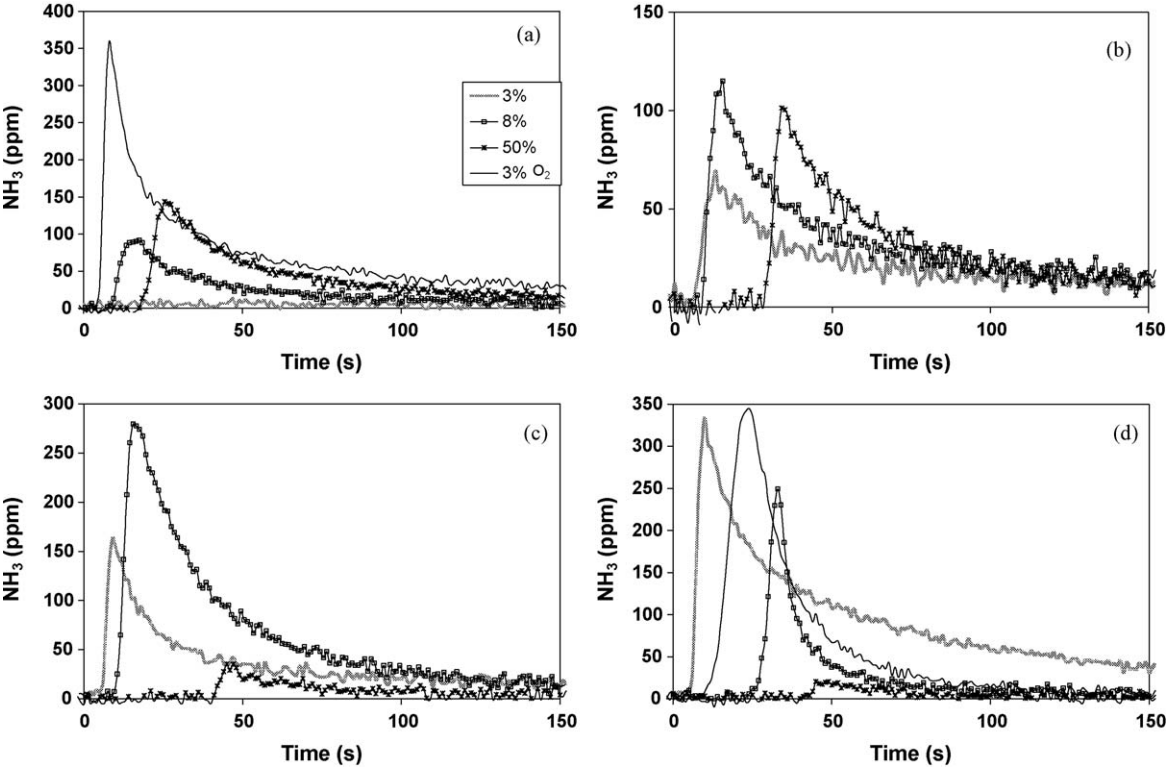

Fig. 11. Effluent NH_3 concentration during the regeneration of a fixed amount of NOx stored (1.5×10^{-5} moles NOx) on the D series catalysts: (a) 160 °C; (b) 230 °C; (c) 300 °C; (d) 370 °C [lean: 500 ppm NO, 5% O_2, balance Ar (varied); rich: 1500 ppm H_2 or 1.15% H_2 and 0.5% O_2, balance Ar (200 s)].

[15,22], or dissociatively adsorbed oxygen [15,20], Pt dispersion clearly has an enhancing effect. As the Pt dispersion is increased for a fixed Pt loading, the length of the Pt/BaO interface increases, providing additional interface for spillover processes to occur. Further, as the Pt dispersion is increased, the exposed Pt surface area (Pt particle size) will increase (decrease), thereby affecting the rate of NO oxidation to NO_2 and correspondingly, the rate of NO_2 storage by disproportionation. At different temperature ranges and times during the regeneration, either the spillover of NOx or the disproportionation mechanism may be the dominant route to NOx storage, which depends on the rate of NO oxidation and the location of the available NOx storage sites.

Depending on the pathway by which NOx is stored (i.e., surface or gas phase transport, involving NO/O_2 or NO_2), the NOx will be stored in different regions of the catalyst defined with respect to the proximity of the storage site (BaO or Al_2O_3) to the precious metal crystallite. Yi et al. [41] concluded that approximately 25% BaO loading is needed to completely cover the Al_2O_3 support. Based on recent NMR studies by Kwak et al. [42], they propose that a special site (5-coordinate Al) on the alumina surface may be required to disperse the BaO and that these sites are only present on about 15–20% of the alumina surface. They also suggest that once this amount of the alumina surface is covered (at a weight loading of about 8–10% BaO), BaO will begin to form multilayers prior to completely covering the Al_2O_3. Given these findings, the 13.0% BaO loading for catalysts D50, D8, and D3 and 16.3% for B3 at a level that a non-negligible fraction of Al_2O_3 is exposed (not covered by BaO) and that the majority of BaO is dispersed on the Al_2O_3. The storage of NOx on γ-Al_2O_3 is possible at low temperatures in the absence of H_2O in the feed and therefore cannot be ruled out [10–14,43]. For feeds containing H_2O, a smaller amount of NOx will store on the Al_2O_3 [44].

It is instructive to propose a schematic showing the different types of barium phase storage sites based on their proximity to Pt crystallites, as shown in Fig. 12. Similar sites presumably exist for the stored NOx on alumina, but are not shown for simplicity. The "proximal region" consists of barium storage sites that are located close to the Pt–BaO interface. The "regenerated region" comprises storage sites that are regenerated during the NOx reduction step. The "bulk region" comprises storage sites further removed from the Pt and also the BaO sites beneath the surface. These bulk region storage sites do not actively participate in the storage process once a cyclic steady-state is reached or in the reduction process before or after a cyclic steady-state is reached. The schematic shown is 2D in order to simplify the picture. Clearly, storage sites can involve solid state diffusional processes [41,45]. Scholz et al. [46,47] described the NOx storage processes as a shrinking or expanding core with surface, semi-bulk, and bulk storage sites. They proposed that the fast uptake of NOx at the beginning of the storage is due to NO adsorption on the surface sites. As the storage proceeds, NOx species diffuse into the barium particles and store on the semi-bulk sites; the bulk storage sites do not participate. Not considered in this picture is that Pt and Ba particles are in intimate contact and that spillover processes are likely. We speculate that for a feed of NO (in O_2), the proximal sites store NOx the fastest, presumably through a spillover process. Once the proximal sites become saturated, the storage slows down because the distance to prospective storage sites increases. If the temperature is sufficient for the NO oxidation to occur, then the NO_2 formed may transport by surface diffusion or gas phase convective diffusion. The latter process makes sites further removed from the Pt more accessible for storage since gas phase transport is typically faster than surface diffusion. As a result, NO_2 will store in the regenerated region and even the surface bulk region, especially if the storage has a sufficient duration.

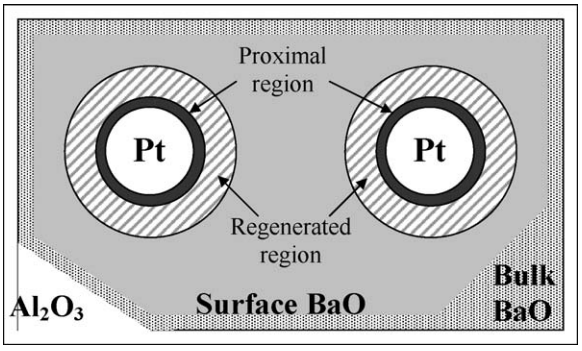

Fig. 12. Schematic diagram showing the different storage regions.

By the end of the storage step, NOx is stored as nitrites and nitrates in the proximal, regenerated, and bulk regions. The relative amount of stored NOx in each of the regions depends on many variables, including the temperature, reductant type, regeneration duration, etc. At low temperatures, the regenerated region is very small, and as the temperature is increased, the size of the regenerated region will increase. As the temperature is increased, the surface species will be able to diffuse a longer distance for a constant regeneration time and therefore, more NOx will be stored and regenerated.

Having defined the local picture of the Pt/BaO catalyst we can now interpret the storage results in more detail. At low temperature (125 °C) and for 60 s storage duration, the data reveal the greatest disparity between the varied dispersion catalysts (in Table 2). Specifically, the ratios ($[NOx\ stored]_{50\%}/[NOx\ stored]_{8\%}$ and $[NOx\ stored]_{8\%}/[NOx\ stored]_{3\%}$) exceed a factor of 2 at 125 °C, decreasing to unity for temperatures exceeding 200 °C. These results suggest that the dominant route to NOx storage is likely through the aforementioned spillover processes. At 125 °C, the rate of NO oxidation is negligible (refer to Fig. 2). Thus, any storage likely involves adsorbed NO, NO_2 and/or O spilling over to the BaO and/or exposed γ-Al_2O_3 phases. As the temperature is increased, the rate of NO oxidation increases, enabling the storage of NOx to occur at an increased rate through gas phase NO_2 transport and subsequent disproportionation chemistry. Indeed, the ratio of NOx stored between the D series catalysts approaches unity at higher temperatures (Table 2). This trend suggests that the dispersion of Pt plays a less significant role in NOx storage at higher temperatures.

The Pt surface area and particle size have an important effect on the NO oxidation rate at moderate to high temperatures (Fig. 2). As expected, the data show that both the NOx storage and NO conversion increase with exposed Pt area. However, a comparison of the D series catalysts to the fourth catalyst (B3), which has a Pt surface area between that of the 50% and 8% Pt dispersion catalysts, indicates that the NO conversion maximum occurs at an intermediate Pt dispersion. Specifically, catalyst B3 resulted in the highest NO conversion at 320 °C in spite of having a lower exposed Pt metal area than catalyst D50 (Table 3). Previously, the rate of NO oxidation on Pt/Al_2O_3 catalysts was shown to increase with Pt particle size for Pt dispersions of 2–7% [26] and for Pt particle sizes (dispersions) of 2.4 nm (42%) and 7 nm (14%) [27]. Olsson and Fridell [26] also examined the rate of NO oxidation on $Pt/BaO/Al_2O_3$ catalysts with varied Pt dispersion (0.6–1%). They reported that an intermediate Pt dispersion catalyst was the most active for NO oxidation. Further, Graham et al. [48] reported that an intermediate Pt and Pt/Pd alloy obtained the highest NO conversion. However, the turnover frequency increased with decreasing Pt dispersion for the Pt dispersions studied. The results reported are consistent with these earlier findings.

Table 3
Maximum NO conversion (to NO_2) as a function of temperature for the D series and B3 catalysts [500 ppm NO, 5% O_2, balance Ar].

Catalyst	Pt atoms exposed ($\times 10^6$) (moles)	Estimated Pt particle size (nm)	Temperature (°C)	NO conversion (%)
B3	3.2	5.2	285 and 320	72.3
D50	8.0	2.2	320	67.5
D8	1.3	12.5	285	62.6
D3	0.5	31.3	285	46.5

4.2. Stored NOx reduction

Previous studies suggest that the reverse spillover of NOx from BaO to Pt [3–8] and the spillover of hydrogen from Pt to BaO [9] are potential mechanisms of stored NOx reduction. A schematic of the spillover of NOx during the storage step and the two spillover processes that are proposed to occur during the regeneration are shown as a schematic in Fig. 13. Fig. 13a shows the Pt crystallites dispersed on the Al_2O_3 support in addition to a BaO particle while Fig. 13b–d is a magnified view of one Pt crystallite on a BaO particle. Fig. 13b conveys that the NO and O_2 fed to the reactor first adsorb on Pt, and then spillover of O, NO, or even NO_2 occurs. The NO_2 produced may also desorb and store further from the Pt particles. In Fig. 13c, H_2 fed to the LNT adsorbs on Pt, scavenging oxygen adatoms and forming vacant Pt sites for proximal stored NOx to spillover [49,50]. The NOx stored further from the Pt interface must diffuse a larger distance to the Pt/BaO interface before it can spillover to Pt. Once the stored NOx spills over onto the Pt particles, hydrogen can react with the NOx forming N_2, N_2O, and NH_3 through conventional Pt-catalyzed chemistry [51]. Another potential pathway is shown in Fig. 13d. After dissociative adsorption of H_2 on Pt, H adatoms first react away any O adatoms as in the previous mechanism. Mobile H may then diffuse to the interface where it may spillover onto the storage phase, partially reducing nitrites and nitrates, forming NO and NO_2. The NO and NO_2 produced will adsorb on Pt and react with hydrogen to form a mixture of N_2, N_2O, and NH_3. Recently, Clayton et al. [33] showed that the NH_3 formed from hydrogen and stored NOx will readsorb on Pt and further react with stored NOx, forming N_2. Similar mechanisms as the ones described in Fig. 13a–d will also occur between Pt particles in contact with the Al_2O_3 support.

The effluent concentration profiles of the reductants (H_2 and NH_3) provide useful information about the regeneration process, reactions occurring, and resulting product distribution. The extent to which kinetic or transport processes limit the rate of stored NOx reduction can be assessed by examining the effluent concentration profiles. At the onset of the regeneration, the catalyst is in the H_2 feed limited state. This state is evidenced by the absence of H_2 in the effluent (complete consumption of H_2) at the beginning of the regeneration (Fig. 10). When reductant breakthrough occurs at an incomplete level of stored NOx conversion, the rate controlling process switches from a feed rate limited state to one in which the transport of stored NOx from the storage sites to the Pt particles (Fig. 13c and d) is limiting [33]. Clayton et al. [33] observed that H_2 and NH_3 breakthrough occurred at higher instantaneous stored NOx conversions as the temperature was increased. Above 275 °C, H_2 and NH_3 break through at nearly complete instantaneous stored NOx conversion.

A comparison of the results for the D series catalysts provides insight about the role of Pt during regeneration. Consider the H_2 breakthrough curves in Fig. 10. Based on the amount of NOx stored (1.1×10^{-5} mole) and the inlet concentration of H_2 (1500 ppm), the breakthrough time for H_2 is estimated to be 34 seconds, assuming that NOx is stored in the form of barium nitrate. However, for the 50% dispersion catalyst, the breakthrough time is observed to be ca. 45 s at 300° C and 47 s at 370 °C (Fig. 10c, 10d). This suggests that H_2 is consumed by species other than stored NOx, the obvious species being chemisorbed oxygen, a product of NO decomposition. The hydrogen oxidation consumes H_2, thus resulting in a delay in the appearance of H_2 in the effluent. This is less important for the lower dispersion catalysts, as we consider in more detail later.

The instantaneous reduction rate can be estimated from the slope of the effluent H_2 concentration profile versus time. At the highest temperature (370 °C), the slope increases with increasing Pt dispersion. These data suggest that the H_2 front moving along the monolith for the high dispersion catalyst (D50) is well-defined and completely regenerates the monolith as it travels through the

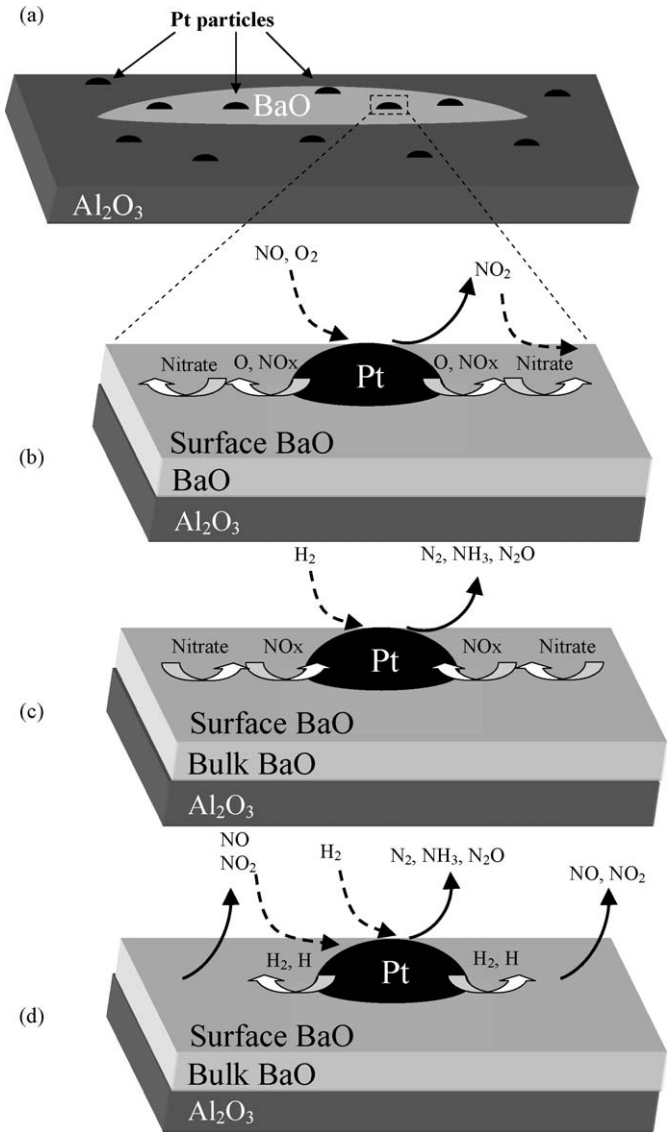

Fig. 13. Schematics of proposed spillover processes: (a) Pt particles dispersed on the Al_2O_3 support and BaO particle; (b) NO, NO_2, and O spillover from Pt to BaO during storage; (c) reverse spillover of NOx from BaO to Pt during regeneration; (d) hydrogen spillover to the storage component to partially reduce the stored NOx.

monolith. On the other hand, the profile is much more gradual for the low Pt dispersion catalyst (D3), suggesting that a well-defined H_2 front does not exist. H_2 breaks through at approximately 6 s and the effluent H_2 concentration does not reach the inlet H_2 concentration until nearly 150 s of regeneration. During the 6–150 s period, H_2 is present throughout the monolith, as is unconverted stored NOx. Under these conditions, the overall regeneration rate becomes limited by the kinetics of spillover of surface species or the diffusion of surface species between the storage component and Pt interface. Whether the spillover involves hydrogen from Pt to the barium phase or stored NOx from barium phase to Pt is unclear. But both require a large Pt/BaO interface in order for the rate of regeneration to increase. Similarly, the surface diffusion of hydrogen or stored NOx both depend on a shorter distance between the storage sites and Pt interface (high Pt dispersion) for an increased rate of regeneration. Since the Pt/BaO interface (average distance between storage sites and Pt interface) is largest (smallest) for the 50% dispersion catalyst, the kinetic limitations are the smallest for this catalyst (Fig. 9).

A plot of the consumption rate of stored NOx to form nitrogen containing species as a function of the instantaneous stored NOx conversion is shown in Fig. 14a. The production rate of stored NOx regenerated is estimated by

$$R(t) = F_{NOx}(t) + F_{NH_3}(t) + 2(F_{N_2}(t) + F_{N_2O}(t)); \quad 0 < t \leq 200 \qquad (8)$$

where $F_i(t)$ are the time dependent effluent molar flow rates of species i. Note that Fig. 14a should be interpreted at different stages of stored NOx conversion, not time; i.e., at a fixed conversion, the time lapsed will be different for each catalyst. The corresponding consumption rate versus time is shown in Fig. 14b. For all the four cases, the production rate increases sharply at the early stage of regeneration. Catalysts D8 and D50 have constant consumption rates until 83% and 95% of the stored NOx is regenerated, respectively (approximately 3.6×10^{-5} moles and 3.0×10^{-5} moles of NOx regenerated per second). At that point, the rate of stored NOx regenerated begins to decrease quickly. The constant rate period corresponds to a pseudo-steady-state during which the H_2 front moves through the monolith. The stored NOx consumption rate is slightly higher for D8 compared to D50 during the period prior to H_2 and NH_3 breakthrough. Fig. 14c compares the effluent N_2 concentrations for the three catalysts at 370 °C. The data suggest that the reduction of stored NOx by intermediate NH_3 is slightly more efficient for D8 than D50. However, for the lowest dispersion catalyst (D3), the rate of stored NOx regeneration is significantly reduced leading to a much earlier breakthrough and inhibition of the ammonia reaction with stored NOx. The aerobic regeneration on catalyst D3 exhibits the highest rate prior to H_2 breakthrough. On the other hand, the anaerobic regeneration on catalyst D3 has the slowest rate and does not reach a pseudo-steady-state during the regeneration because of larger spillover limitations likely due to the smaller Pt/BaO interface.

The maximum N_2 concentration achieved by the three catalysts provides insight about the reactions occurring during the regeneration. If H_2 completely reacts with $Ba(NO_3)_2$, then 5 moles of H_2 will produce 1 mole of N_2. With the anaerobic feed containing 1500 ppm H_2, this would result in a effluent containing 300 ppm N_2. The D3 catalyst nearly achieves this upper limit (Fig. 14c). In contrast, the peak N_2 concentration for the D8 and D50 catalysts are somewhat lower (280 and 250 ppm, respectively). This reduced N_2 peak concentration is attributed to the consumption of H_2 with oxygen adsorbed on Pt. This reaction is more significant as the exposed Pt area increases.

The rate of NOx transported to Pt from BaO will affect the speed and shape of the H_2 front and the amount of NOx that is regenerated after H_2 breaks through. The distance from which the

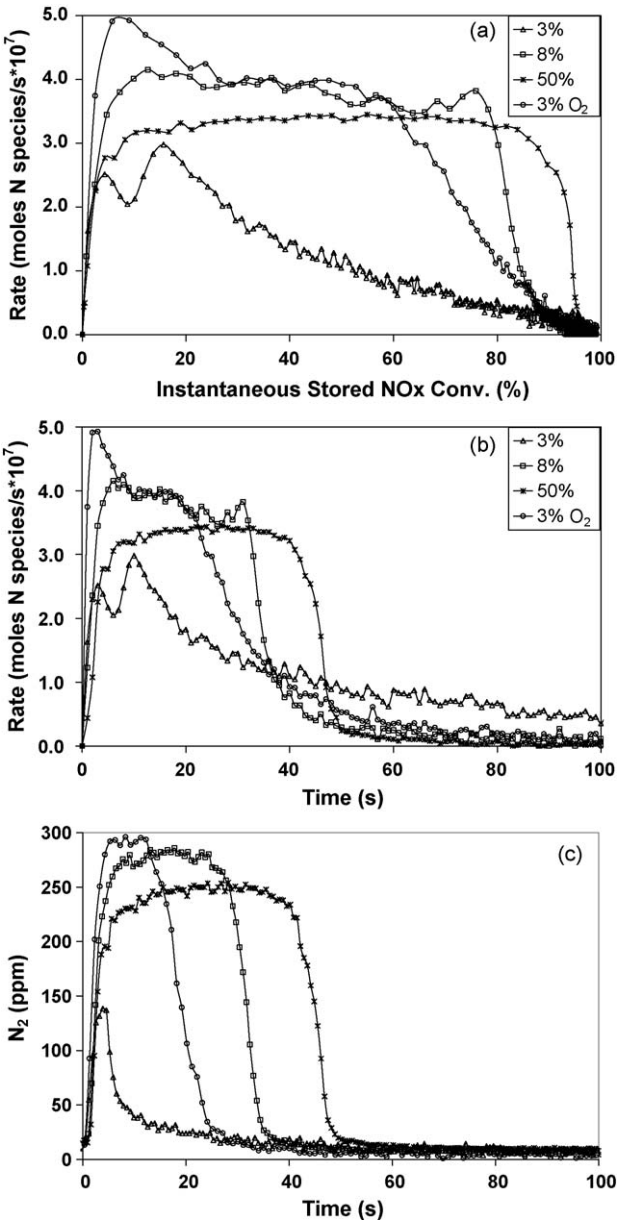

Fig. 14. Production rate of stored NOx regenerated forming nitrogen containing species that are measured in the effluent for a fixed amount of NOx stored (1.5×10^{-5} moles NOx) versus (a) the instantaneous stored NOx conversion and (b) time; for the D series catalysts at 370 °C; (c) effluent N_2 concentration versus time [lean: 500 ppm NO, 5% O_2, balance Ar (varied); rich: 1500 ppm H_2 or 1.15% H_2 and 0.5% O_2, balance Ar (200 s)].

NOx is stored to the Pt/BaO interface (Pt dispersion) affects the average rate of NOx transported to Pt from BaO. As the Pt dispersion is decreased for fixed Pt and BaO loadings, the average distance of stored NOx from the Pt/BaO interface increases. NOx stored in close proximity to the Pt/Ba interface will react on Pt quickly, while NOx stored further from Pt will require longer time to transport to the Pt and react. As seen in Fig. 9a–d, the amount of stored NOx regenerated during the anaerobic regenerations increases with increased Pt dispersion. This is consistent with a decrease in the average distance between BaO and the Pt/BaO interface. At 370 °C, all the three catalysts exhibited nearly complete stored NOx conversion prior to the end of the anaerobic regenerations. However, catalyst D3 regenerated the stored NOx much slower, suggesting a rate limitation involving the reverse spillover of stored NOx to Pt or of adsorbed hydrogen from Pt to

Table 4
Estimated percent age of stored NOx conversion before and after H_2 breakthrough for the D series catalysts [lean: 500 ppm NO, 5% O_2, balance Ar (varied); rich: 1500 ppm H_2 or 1.15% H_2 and 0.5% O_2 balance Ar (200 s)].

Temperature (°C)	Percent age of stored NOx converted before and after H_2 breakthrough							
	D3		D8		D50		D3 O_2	
	Before	After	Before	After	Before	After	Before	After
160	17	83	13	87	38	63	9	91
230	15	85	37	63	68	32	–	–
300	17	83	36	64	93	7	–	–
370	8	92	77	23	95	5	54	46

BaO. In Fig. 10d, the shape of the effluent H_2 profile for catalyst D3 (anaerobic regeneration) increased more gradually after H_2 breakthrough, unlike the sharp increase observed for the higher dispersion catalysts (D8 and D50). This further suggests that a rate limitation exists that is much more dominant in the low dispersion catalysts.

Some of the contributing factors of the observed trends in NH_3 production are analyzed here for the fixed NOx storage experiments. As reported in Fig. 7, the net production of NH_3 is maximized in different temperature ranges depending on the Pt dispersion. The NH_3 selectivity results (Fig. 6) and estimates for the percent age of stored NOx converted before and after H_2 breakthrough (Table 4) indicate that the selectivity to NH_3 increases as the percentage of stored NOx regenerated after H_2 breakthrough increases. This is consistent with our understanding of the chemistry in the presence and absence of gas phase H_2. Fig. 5 shows that NH_3 breaks through at about the same time as H_2 which results in a rapid decrease in the production of N_2. After H_2 breaks through, the entire monolith is exposed to H_2. This creates conditions that are favorable for NH_3 formation. Clayton et al. [51] reported that H_2 inhibits the reaction between NH_3 and NO and the decomposition of NH_3 under steady-state conditions. They showed that the addition of H_2 to a feed of NO and NH_3 maintained 100% conversion of NO and H_2 while the conversion of NH_3 decreased as the H_2 concentration was increased.

These results, taken together, suggest that the overall rate of NOx transported to Pt from the barium storage sites is critical in affecting the net production of NH_3. In the feed rate limited state, the rate of stored NOx transport to Pt is fast compared to the H_2 feed rate. Under these conditions, a well-defined H_2 front will form with the overall chemistry having a parallel-consecutive structure in which N_2 is formed directly or indirectly through NH_3:

$$\text{Direct}: H_2 + NOx \rightarrow N_2$$

$$\text{Indirect}: H_2 + NOx \rightarrow NH_3; NH_3 + NOx \rightarrow N_2$$

The formation of NH_3 is rapid under anaerobic conditions as the high H_2/NOx is favorable for NH_3 generation on Pt [10,36]. The difference in observed NH_3 selectivities is primarily affected by the rate of ammonia reaction with stored NOx. Once H_2 breaks through, only a relatively small fraction of stored NOx remains to produce NH_3. On the other hand, if the rate of stored NOx transported to Pt is slower than the H_2 feed rate, then H_2 will break through with substantially more stored NOx remaining on the catalyst after H_2 breakthrough. As a result, the Pt surface will be predominantly covered by hydrogen, and as the stored NOx transports to the Pt particles, NH_3 will be formed. As described earlier, this ammonia does not effectively react with stored NOx under these net reducing conditions. Thus, the reduced rate of NOx regeneration on the low dispersion catalyst leads to conditions that inhibit the consumption of the NH_3 intermediate.

In some of the experiments carried out, the initial amount of NOx stored was fixed by design (Figs. 5–11). However, the types of NOx stored are not identical, which may affect the rate of NOx transport from the BaO storage phase to Pt. For example, more stable stored NOx (NOx stored at higher temperatures as nitrates) may react slower. Nova et al. [52] showed that storing NOx at 200 °C and regenerating at 200 °C or lower (150 °C and 100 °C) produced more NH_3 as the temperature was decreased. This method of storing NOx at a fixed temperature and then decreasing the temperature may have similar types of stored NOx, however, the loosely bound NOx can desorb when the feed gas is switched to an inert feed (Ar only). This stored NOx contributes to the formation of the NOx "puff" and N_2O (Fig. 14) at the beginning of the regeneration and therefore is not observed [52]. Controlling the types and amount of stored NOx for different catalysts is very difficult and was not attempted here.

A comparison of the aerobic (Figs. 3 and 4) and anaerobic (Fig. 6) regeneration feeds shows similar NOx conversion and selectivity trends for the varied dispersion catalysts. One interesting trend is that the net production of NH_3 was maximized by each of the three catalysts in different temperature ranges. These findings are important for LNT/SCR systems in which production of NH_3 in the LNT should be maximized. While the trends are similar for the aerobic and anaerobic regeneration feeds (Figs. 3 and 6), the data cannot be compared in detail due to several complicating factors encountered during regeneration. These include the amount of NOx stored before regeneration, the amount of excess H_2, the duration of the regeneration step, the temperature rise due to hydrogen oxidation, and the amount of H_2O formed. For this reason, experiments were designed to limit the differences between the aerobic and anaerobic regenerations to only the exotherm and H_2O formed by the oxidation of H_2 with feed O_2 during the aerobic regeneration. This was accomplished by comparing equal amounts of excess H_2 (Fig. 6c, 160 °C and 370 °C) and nearly equal amounts of stored NOx (approximately 1.5×10^{-5} moles) and is discussed next.

A comparison of the anaerobic and aerobic feeds for catalyst D3 for the same feed temperature 370 °C (Fig. 6c) shows comparable NOx conversions (96% and 89%). However, the product selectivities are quite different; the anaerobic feed resulted in an NH_3 selectivity of 84% while the aerobic feed gave a NH_3 selectivity of only 51%. On the other hand, at the lower feed temperature of 160 °C, while the product selectivities were similar, the NOx conversions were quite different, 11% versus 63% for the anaerobic and aerobic regeneration feeds, respectively. The higher NOx conversion obtained with the aerobic feed suggests that the exotherm and/or H_2O formed from the oxidation of H_2 are beneficial at the lower feed temperature in increasing the amount of stored NOx that is regenerated. Epling et al. [53] reported that the addition of O_2 during the regeneration enhanced the performance of the NSR catalyst below 375 °C. They attributed the enhancement to increased trapping during the subsequent storage step due to the temperature rise from the reductant oxidation, which enhances the conversion of NO to NO_2. The effect of added O_2 during the regeneration was reported to decrease formation of NH_3 at 375 °C and increase its formation at 288 °C while keeping excess reductant available for NOx reduction

constant [53]. The results (Fig. 7) suggest that the large exotherm produced from adding O_2 to the regeneration, causes an increased rate of regeneration, which affects the product selectivity.

The importance of the added O_2 during the regeneration and the effect of Pt dispersion are discussed here for NOx stored in the absence of H_2O. A comparison of the aerobic regeneration feed with a low Pt dispersion catalyst (3%) to the highly dispersed Pt catalyst (D50) without O_2 fed during the regeneration (equal NOx stored and excess H_2) at 160 °C (Figs. 6c and 9a) shows that the lower dispersion catalyst was able to regenerate more stored NOx. This suggests that the exotherm (Fig. 8) and/or H_2O formed during the regeneration are more important at lower temperatures than the larger Pt surface area and Pt/BaO interface for regenerating stored NOx. On the other hand, at higher temperature (370 °C), catalyst D50 (anaerobic) and D3 (aerobic and anaerobic) regenerate nearly the same amount of stored NOx during the 200 s regeneration. However, catalyst D3 (anaerobic) regenerated the stored NOx under anaerobic conditions much slower than under aerobic conditions. This suggests that the effect of the exotherm and H_2O produced during the regeneration is still beneficial at higher temperatures. Lietti et al. [54] observed an increase in the NOx reduction efficiency at lower temperatures when adding 1% H_2O to the regeneration feed (2000 ppm H_2) after storing NOx in a dry feed (1000 ppm NO and 3% O_2). Their results are consistent with our findings, although our results have the additional effect of the exotherm from H_2 oxidation. The effect of the exotherm and H_2O produced during the regeneration should be decoupled to pinpoint the cause of the enhancement. These studies are underway and will be published elsewhere.

5. Conclusions

The Pt dispersion was observed to affect many aspects of the NOx storage and reduction performance of $Pt/BaO/Al_2O_3$ monoliths. Below 200 °C, the differences in storage and reduction activity were the largest between the varied Pt dispersion catalysts (3%, 8%, and 50%). The amount of NOx stored increased with increased dispersion for the temperature range studied (125–340 °C). The increased storage is attributed to the larger Pt surface area and Pt/BaO interfacial perimeter, which enhances the spillover of NOx from Pt to BaO. During the regeneration, the amount of stored NOx that is reduced increased with increasing Pt dispersion for a fixed amount of NOx stored. At 370 °C, the stored NOx was almost completely regenerated for the three catalysts. However, the regeneration of the 3% dispersion catalyst was much slower. This suggests that a kinetic process such as the reverse spillover of stored NOx or the spillover of hydrogen from Pt to BaO may limit the overall rate. Moreover, since the average distance of the storage sites to the Pt/BaO interface is the largest for the 3% dispersion catalyst, this suggests that the transport of surface species between the storage sites and Pt particles may limit the rate.

The Pt dispersion had a significant effect on the product distribution. For the aerobic regeneration feed, the most net NH_3 was generated by the 50% dispersion catalyst at the lowest temperature (125 °C), by the 3% dispersion catalyst at the highest temperature (340 °C), and by the 8% dispersion catalyst at the intermediate temperatures (170–290 °C). Similar trends were observed for the net production of NH_3 with an anaerobic regeneration feed. The trends in N_2 and N_2O production for the aerobic regeneration feed were similar for the varied dispersion catalysts over the temperature range studied. However, the extent of the production of N_2 and N_2O was substantially different due to different amounts of stored NOx being regenerated.

A comparison of an aerobic and anaerobic regeneration feed with equal amounts of excess H_2 and stored NOx was investigated on a 3% Pt dispersion catalyst. The NOx conversions at low temperatures (160 °C) and product selectivities at high temperatures were extremely different with aerobic and anaerobic regeneration feeds. The conversion results suggest that the exotherm and/or H_2O formed from H_2 oxidation are beneficial at low feed temperature for increasing the amount of stored NOx that is regenerated.

In this study, we have gained insight into the effect of Pt dispersion on the product distribution during NOx storage and reduction. The results show that the catalyst properties can be optimized to produce NH_3 rather than N_2 for the LNT/SCR systems or oppositely, to minimize the net NH_3 production if a SCR catalyst is not used downstream of the LNT. This can be exploited to maximize the performance of these aftertreatment devices.

Acknowledgements

The work reported was supported by the U.S. DOE National Energy Technology Laboratory (DE-FC26-05NT42630) and the Texas Hazardous Waste Reduction Center. We also acknowledge BASF Catalysts LLC for providing the catalysts used in this study.

References

[1] I. Nova, L. Lietti, L. Castoldi, E. Tronconi, P. Forzatti, Journal of Catalysis 239 (1) (2006) 244–254.
[2] I. Nova, L. Castoldi, L. Lietti, E. Tronconi, P. Forzatti, Society of Automotive Engineers [Special Publication] SP SP-2022 (2006) 397–406 (Diesel Exhaust).
[3] N.W. Cant, I.O.Y. Liu, M.J. Patterson, Journal of Catalysis 243 (2) (2006) 309–317.
[4] D. James, E. Fourre, M. Ishii, M. Bowker, Applied Catalysis B: Environmental 45 (2) (2003) 147–159.
[5] L. Olsson, H. Persson, E. Fridell, M. Skoglundh, B. Andersson, Journal of Physical Chemistry B 105 (2001) 6895–6906.
[6] J.A. Anderson, B. Bachiller-Baeza, M. Fernandez-Garcia, Physical Chemistry Chemical Physics 5 (2003) 4418–4427.
[7] G. Zhou, T. Luo, R.J. Gorte, Applied Catalysis B: Environmental 64 (1–2) (2006) 88–95.
[8] A. Scotti, I. Nova, E. Tronconi, L. Castoldi, L. Lietti, P. Forzatti, Industrial & Engineering Chemistry Research 43 (16) (2004) 4522–4534.
[9] Z. Liu, J.A. Anderson, Journal of Catalysis 224 (1) (2004) 18–27.
[10] R.D. Clayton, M.P. Harold, V. Balakotaiah, AIChE Journal 55 (2009) 687–700.
[11] A. Lindholm, N.W. Currier, E. Fridell, A. Yezerets, L. Olsson, Applied Catalysis B: Environmental 75 (1–2) (2007) 78–87.
[12] A.J. Paterson, D.J. Rosenberg, J.A. Anderson, Studies in Surface Science and Catalysis 138 (2001) 429–436 (spillover and mobility of species on solid surfaces).
[13] F. Prinetto, G. Ghiotti, I. Nova, L. Lietti, E. Tronconi, P. Forzatti, Journal of Physical Chemistry B 105 (2001) 12732–12745.
[14] B. Westerberg, E. Fridell, Journal of Molecular Catalysis A: Chemical 165 (1–2) (2001) 249–263.
[15] K.S. Kabin, P. Khanna, R.L. Muncrief, V. Medhekar, M.P. Harold, Catalysis Today 114 (1) (2006) 72–85.
[16] L. Olsson, H. Persson, E. Fridell, M. Skoglundh, B. Andersson, Journal of Physical Chemistry B 105 (29) (2001) 6895–6906.
[17] E. Fridell, H. Persson, L. Olsson, B. Westerberg, A. Amberntsson, M. Skoglundh, Topics in Catalysis 16/17 (1–4) (2001) 133–137.
[18] W.S. Epling, L.E. Campell, A. Yezerets, N.W. Currier, J.E. Parks, Catalysis Reviews 46 (2) (2004) 163–245.
[19] Kabin, K.S., NOx Storage and Reduction Studies on Pt/Ba/Alumina Monolithic Catalysts, Ph.D. Dissertation, University of Houston, 2005.
[20] W.S. Epling, J.E. Parks, G.C. Campbell, A. Yezerets, N.W. Currier, L.E. Campbell, Catalysis Today 96 (1–2) (2004) 21–30.
[21] E. Fridell, M. Skoglundh, B. Westerberg, S. Johansson, G. Smedler, Journal of Catalysis 183 (1999) 196–209.
[22] I. Nova, L. Castoldi, L. Lietti, E. Tronconi, P. Forzatti, F. Prinetto, G. Ghiotti, Journal of Catalysis 222 (2) (2004) 377–388.
[23] F. Prinetto, G. Ghiotti, I. Nova, L. Castoldi, L. Lietti, E. Tronconi, P. Forzatti, Physical Chemistry Chemical Physics 5 (2003) 4428–4434.
[24] J.I. Theis, U. Gobel, M. Kogel, T.P. Kreuzer, D. Lindner, E. Lox, L. Ruwisch, Society of Automotive Engineers [Special Publication] SP SP-1676 (2002) 1–9 (Emissions Modeling and General Emissions).
[25] Y.O.K. Sakamoto, Y. Kizaki, S. Matsunaga, N. Takahashi, H. Shinjoh, Journal of Catalysis 238 (2) (2006) 361–368.
[26] L. Olsson, E. Fridell, Journal of Catalysis 210 (2) (2002) 340–353.
[27] S.S. Mulla, N. Chen, L. Cumaranatunge, G.E. Blau, D.Y. Zemlyanov, W.N. Delgass, W.S. Epling, F.H. Ribeiro, Journal of Catalysis 241 (2) (2006) 389–399.
[28] P. Denton, A. Giroir-Fendler, H. Praliaud, M. Primet, Journal of Catalysis 189 (2) (2000) 410–420.
[29] J.-H. Lee, H.H. Kung, Catalysis Letters 51 (1,2) (1998) 1–4.

[30] E. Xue, K. Seshan, J.R.H. Ross, Applied Catalysis B: Environmental 11 (1) (1996) 65–79.
[31] A. Lindholm, N.W. Currier, J. Dawody, A. Hidayat, J. Li, A. Yezerets, L. Olsson, Applied Catalysis B: Environmental 88 (2009) 240–248.
[32] S.Y. Christou, A.M. Efstathiou, Topics in Catalysis 42/43 (2007) 351–355.
[33] R.D. Clayton, M.P. Harold, V. Balakotaiah, Applied Catalysis B: Environmental 84 (2008) 616–630.
[34] R.D. Clayton, Ph.D. Dissertation, University of Houston, Steady-State and Cyclic Studies of $Pt/BaO/Al_2O_3$ Lean NOx Traps (2008).
[35] K.S. Kabin, R.L. Muncrief, M.P. Harold, Catalysis Today 96 (1–2) (2004) 79–89.
[36] J. Xu, R.D. Clayton, V. Balakotaiah, M.P. Harold, Applied Catalysis B: Environmental 77 (2008) 395–408.
[37] R. Muncrief, P. Khanna, K. Kabin, M.P. Harold, Catal. Today 98 (2004) 393–402.
[38] J.R. Theis, E. Gulari, Applied Catalysis B: Environmental 75 (1–2) (2007) 39–51.
[39] M. Sharma, M.P. Harold, V. Balakotaiah, Industrial and Engineering Chemistry Research 44 (2005) 6264–6277.
[40] J. Xu, M.P. Harold, V. Balakotaiah, Applied Catalysis B: Environmental (2008), doi:10.1016/j.apcatb.2008.11.017.
[41] C.-W. Yi, J.H. Kwak, J. Szanyi, Journal of Physical Chemistry C 111 (42) (2007) 15299–15305.
[42] J.H. Kwak, J.Z. Hu, D.H. Kim, J. Szanyi, C.H.F. Peden, Journal of Catalysis 251 (1) (2007) 189–194.
[43] R.L. Muncrief, K.S. Kabin, M.P. Harold, AIChE Journal 50 (10) (2004) 2526–2540.
[44] T.J. Toops, D.B. Smith, W.S. Epling, J.E. Parks, W.P. Partridge, Applied Catalysis B: Environmental 58 (3–4) (2005) 255–264.
[45] U. Tuttlies, V. Schmeisser, G. Eigenberger, Chemical Engineering Science 59 (22–23) (2004) 4731–4738.
[46] C.M.L. Scholz, V.R. Gangwal, M.H.J.M. de Croon, J.C. Schouten, Journal of Catalysis 245 (1) (2007) 215–227.
[47] C.M.L. Scholz, K.M. Nauta, M.H.J.M. de Croon, J.C. Schouten, Chemical Engineering Science 63 (11) (2008) 2843–2855.
[48] G.W. Graham, H.W. Jen, O. Ezekoye, R.J. Kudla, W. Chun, X.Q. Pan, R.W. McCabe, Catalysis Letters 116 (1–2) (2007) 1–8.
[49] V. Medhekar, V. Balakotaiah, M.P. Harold, Catalysis Today 121 (3–4) (2007) 226–236.
[50] A. Kumar, V. Medhekar, M.P. Harold, V. Balakotaiah, Applied Catalysis B: Environmental, in press, doi:10.1016/j.apcatb.2009.04.027.
[51] R.D. Clayton, M.P. Harold, V. Balakotaiah, Applied Catalysis B: Environmental 81 (2008) 161–181.
[52] I. Nova, L. Lietti, P. Forzatti, Catalysis Today 136 (1–2) (2008) 128–135.
[53] W.S. Epling, D. Kisinger, C. Everest, Catalysis Today 136 (1–2) (2008) 156–163.
[54] L. Lietti, I. Nova, P. Forzatti, Journal of Catalysis 257 (2) (2008) 270–282.